JOURNAL OF THE ROYAL SOCIETY Interface

Hysteresis of soft joints embedded with fluid-filled microchannels

Animangsu Ghatak, Abhijit Majumder and Rajendra Kumar

J. R. Soc. Interface 2009 **6**, 203-208
doi: 10.1098/rsif.2008.0180

JOURNAL OF THE ROYAL SOCIETY Interface

J. R. Soc. Interface (2009) **6**, 203–208
doi:10.1098/rsif.2008.0180
Published online 8 July 2008

Hysteresis of soft joints embedded with fluid-filled microchannels

Animangsu Ghatak*, Abhijit Majumder and Rajendra Kumar

Department of Chemical Engineering, Indian Institute of Technology, Kanpur 208 016, India

Many arthropods are known to achieve dynamic stability during rapid locomotion on rough terrains despite the absence of an elaborate nervous system. While muscle viscoelasticity and its inherent friction have been thought to cause this passive absorption of energy, the role of embedded microstructures in muscles and muscle joints has not yet been investigated. Inspired by the soft and flexible hinge joints present in many of these animals, we have carried out displacement-controlled bending of thin elastic slabs embedded with fluid-filled microchannels. During loading, the slab bends uniformly to a critical curvature, beyond which the skin covering the channel buckles with a catastrophic decrease in load. In the reverse cycle, the buckled skin straightens out but at a significantly lower load. In such a loading–unloading cycle, this localized buckling phenomenon results in a dynamic change in the geometry of the joint, which leads to a significant hysteresis in elastic energy. The hysteresis varies nonlinearly with channel diameters and thicknesses of the slab, which is captured by a simple scaling analysis of the phenomenon.

Keywords: soft joint; microchannel; hysteresis; buckling instability

1. INTRODUCTION

The mechanisms by which many arthropods dart on uneven and rough terrains and yet maintain stability have attracted the attention of naturalists, biologists and engineers alike (Ting *et al.* 1994; Gronenberg 1996; Full & Koditschek 1999). Because while vertebrates and others have developed an elaborate response mechanism, e.g. 'reflex' action to take care of dynamic stability, these insects must employ a passive damping system for rapid absorption of energy caused by eventual shocks during locomotion (Dudek & Full 2006). Similarly, many flying insects should not only flap their wings at an exceptionally high rate (Grodnitsky 1999) but also guard against unwanted circumstances such as eddy turbulent wind, transition from hovering to flapping mode and even faulty flapping of their own wings (Gorb 1999*a*; Sane *et al.* 2007). Rapid actions of these types demand the presence of elastic tissues in the associated limbs as is indeed found in the form of resiline, a rubber-like protein, e.g. in flight muscles of dragonfly (Andersen & Weis-Fogh 1964), jumping system of locusts and beetles (Bennet-Clark 1975; Furth *et al.* 1983; Furth & Suzuki 1992), wing folding mechanism of earwigs (Haas *et al.* 2000) and vein joints of damselfly (Dudek & Full 2006). However, these muscles have additional functions so that their geometry and internal structure must involve designs that can reduce fatigue during cyclic loading–unloading and, importantly, can act as dampers for fluctuating loads including sudden shocks. Several mechanisms have been thought to implement such passive absorption of energy: interlayer friction at movable joints (Gorb 1999*b*; Dai *et al.* 2006); muscle viscoelasticity; and spring–mass arrangements (Dudek & Full 2006). While these methods can cause continuous modulation of perturbations promoting better manoeuvrability and control, they are detrimental for the rapid movement that these joints are designed to perform and inadequate for responding to shocks that require the damping mechanism to trigger only beyond a critical load. Besides, in many insects, damping is independent of the rate of loading, contrary to what is achieved by these mechanisms. In this context, we show here that the internal microstructures, e.g. air pockets and fluid-filled chambers in soft joints, as depicted by the leg of a locust in figure 1, can cause significant energy absorption and damping when deformed beyond a critical limit. While the role of such subsurface microstructures has earlier been recognized in the context of adhesion and the gripping mechanisms for many of these animals (Gillett & Wigglesworth 1932; Majumder *et al.* 2007), their influence on dynamic stability during terrestrial locomotion or aerial flight has not yet been known. We have mimicked these soft joints by preparing thin elastomeric slabs embedded with microchannels. We have performed systematic bending experiments on these slabs to show that when a critical curvature is reached, localized buckling occurs in the vicinity of the channel, which leads to the formation of a kink. The kink then acts as a hinge for further bending of the slab. In the reverse cycle as the load is gradually withdrawn, the kink disappears although at a significantly smaller load

*Author for correspondence (aghatak@iitk.ac.in).

Received 4 May 2008
Accepted 16 June 2008

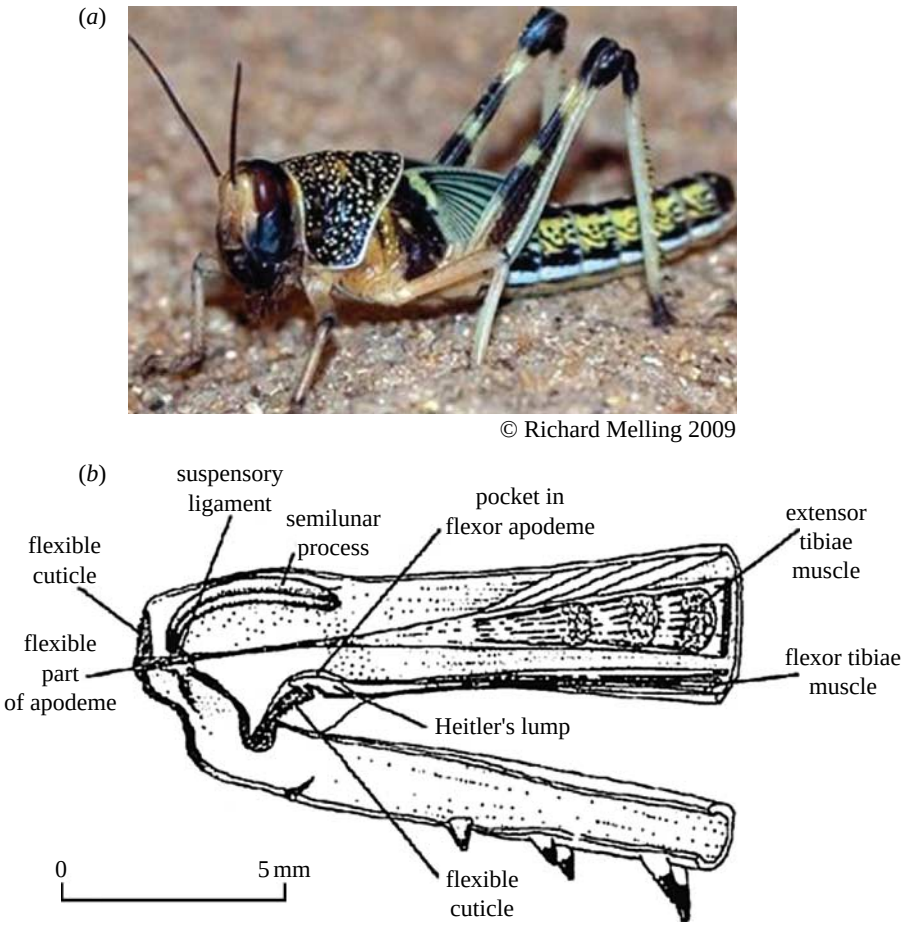

Figure 1. (*a*) Locust and (*b*) the simplified internal anatomy of its leg (adapted from fig. 1 on p. 6 of Bennet-Clark (1975)) showing the fluid-filled chamber in the leg including at the joint between the femur and tibia.

resulting in hysteresis. Looking at the possibility of using these microstructure-embedded joints for designing soft robotic arms (Shimoyama *et al.* 1993), flexible actuators, compliant load-bearing elements, prosthetic elements, components of microfluidic devices and diagnosis and treatment of musculoskeletal diseases (Hyon *et al.* 2007), we have systematically investigated this phenomenon. We have varied the geometric parameters of the joint, the rate at which it is loaded and the viscosity of the liquid used to fill the channels. These results show that not only geometry but also dynamic change in the geometry during cyclic loading and unloading lead to the hysteresis and passive absorption of energy.

2. EXPERIMENTAL

Figure 2*a* shows the three-dimensional view of a typical elastic rectangular slab made of cross-linked polydimethylsiloxane (PDMS), in which an embedded channel of circular cross section spans along its width. These samples were prepared by pouring Sylgard 184 elastomer mixed with a curing agent (10 : 1 by weight) between two silanized glass slides that were kept separated by two spacers of desired height. For generating the channel, a solid rod was used as the template, which was immersed in the pool of pre-cross-linked liquid (Verma *et al.* 2006). After curing the elastomer at 80°C for an hour, it was swelled in chloroform, following which the rod was gently pulled out of the swollen block to generate the channel; the block was then de-swelled by slowly drying the solvent. The cross-linked network thus prepared was elastic with its storage modulus two orders of magnitude larger than the loss modulus (Ghatak *et al.* 2005). While in most of our experiments, the channel was located at the middle of the slab (skin thickness $t_1 = t_2$), its vertical location within the layer could be varied by suitably positioning the template. The two ends of the slab were supported on two rigid plates with its middle portion hanging in between such that the channel was placed at equal distance $L/2$ from these supports. In order to prevent slippage, the slab was strongly attached to the supports using an adhesive tape and was then subjected to bending, as shown in figure 2*b*. Initial bending of the slab occurred by the dead weight of the top plate, which was then further pushed vertically down at a constant rate using a motorized micromanipulator. The vertical displacement Δ of the point of application of the load was measured with respect to this initial bent state of the slab, while the applied load F was obtained using a load cell interfaced with a computer. The extent of bending was estimated using a video camera that captured the side view of the slab.

3. RESULTS AND DISCUSSION

Curve a in figure 2*k* represents a typical F versus Δ plot obtained when an elastic slab without any embedded structure is progressively bent; no hysteresis is observed

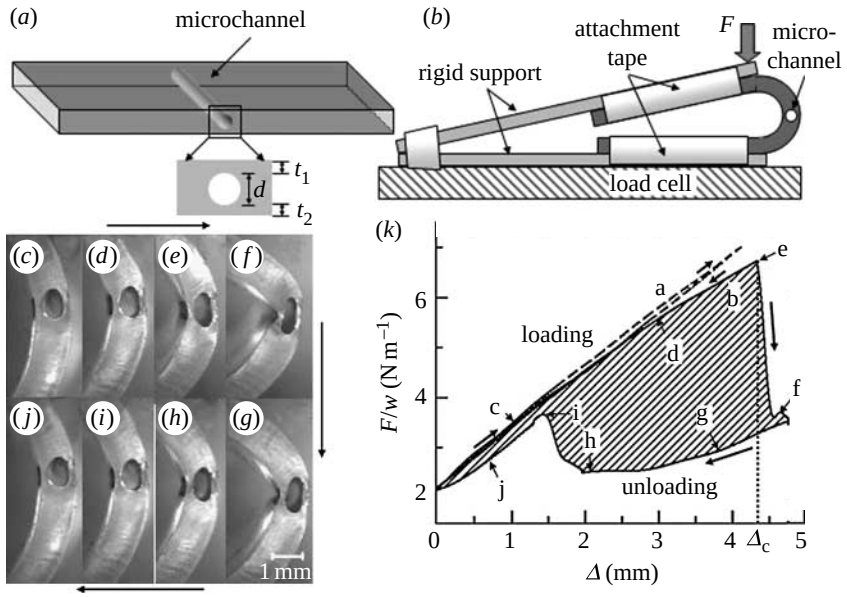

Figure 2. Schematic of the experiment. (*a*) The three-dimensional view of a thin elastic rectangular slab of PDMS in which a circular channel is embedded at various vertical locations. The slab is supported on two rigid plates at two of its ends while the middle portion with the channel at the centre hangs unsupported. (*b*) The slab is bent between these two plates with the bottom plate remaining fixed on a load cell interfaced with a computer. In a displacement-controlled experiment, the top plate is pushed down using a micromanipulator while the load cell is used to record the dynamic load. (*c–h*) The video micrographs depict the side view of a slab in a typical loading–unloading experiment. In this sequence, with progressive increase in load (*c–e*), bending of the slab increases while the circular channel ovalizes. Finally, (*e*) a critical curvature is reached, at which the thin skin in the compressed side of the slab buckles inwards to form a (*f*) kink. In the reverse cycle, as the load is gradually withdrawn, (*h*) the fold eventually straightens out but at a load much smaller than that at which it appeared. (*k*) Load versus displacement curve obtained from a typical loading–unloading experiment using an elastic slab (curve a) of thickness $h=1300$ μm and with no embedded channel, and an elastic slab (curve b) of thickness $h=1300$ μm, length $L=20$ mm and channel diameter $d=800$ μm. In the forward cycle, the kink appears with a catastrophic decrease in load at a threshold displacement Δ_c, while in the reverse cycle it disappears at a load and displacement which are smaller than that at which the kink appears.

during loading and unloading. Similar observation is also made for a slab with an embedded channel having a channel diameter d smaller than a critical value $d< d_c$. The slab bends uniformly at both its inner and outer sides. However, when the diameter of the channel exceeds the critical diameter, $d> d_c$, bending does not proceed uniformly; instead, beyond a critical curvature, i.e. radius of curvature ρ less than a critical value ρ_c, the compression at the inner side results in the buckling of the thin skin that folds inside the channel with the appearance of a kink. Concomitant to that, in the force–displacement plot (curve b, figure 2*k*), the bending force decreases catastrophically to a lower value. Following this buckling instability, the kink acts as a hinge so that further bending requires significantly smaller loads to be applied. Figure 2*c–f* shows a sequence of video micrographs of the side view of the samples, in which the circular hole first ovalizes and then folds inwards owing to buckling of the skin over it. In the reverse cycle, as the applied load is progressively withdrawn, the folded skin eventually straightens out (micrographs, figure 2*g–j*) but at a load much smaller than that at which it initially buckled. In fact, the unloading part of a typical force–displacement plot shows a non-monotonic behaviour. With a decrease in Δ, the load first decreases (from f→h), then increases (from h→i) to coincide with the loading curve and finally decreases with a slope similar to the loading curve (i→j). The portion of the unloading curve i→j however does not coincide completely with the loading curve for all slabs. The hysteresis in elastic energy is estimated from the shaded area in the load–displacement plot as depicted in figure 2*k*.

The loading–unloading cycle was systematically studied in figure 3, in which both the geometric feature of the joint and the dynamics of the experiment were examined. Figure 3*a* depicts the change in the loading and unloading history for elastic slabs of varying thickness, $h=1240$, 1340, 1800 and 2140 μm, but of common channel diameter $d=800$ μm. Curve 1, representing $d/h=0.37$, shows that when the channel diameter is too small, i.e. the skin is too thick to undergo local buckling, the loading and unloading data superimpose exhibiting negligible hysteresis. However, for $d/h\sim0.44$ (curve 2), beyond a threshold displacement during loading, the load decreases to a lower value, albeit not catastrophically but gradually, which signifies that a sharp kink does not appear instantly for this film. In the regime i–j, the unloading curve does not fully coincide with the loading curve because, possibly, of the inherent viscoelasticity of the material, which becomes more prominent for thick slabs. As the d/h ratio is increased to 0.6 as in curve 3, F decreases catastrophically beyond a threshold Δ_c; here also we see considerable hysteresis in the reverse cycle. With further increase in d/h, hysteresis decreases and becomes almost imperceptible in the limit of $d/h\sim0.65$. In essence, kinking instability

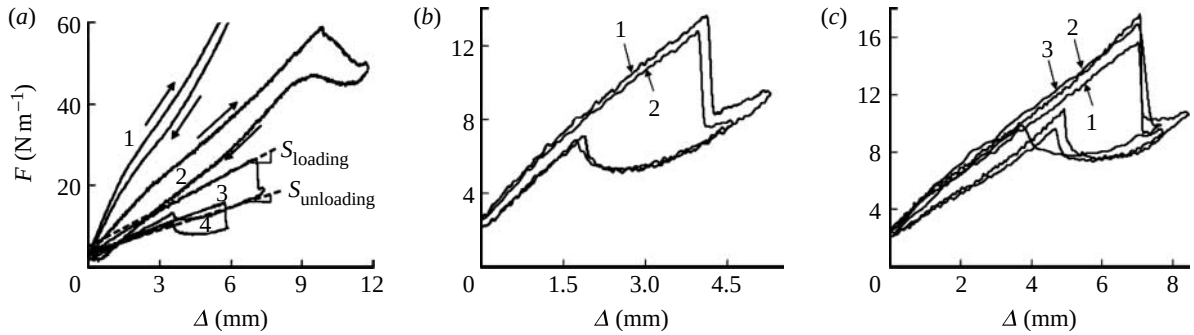

Figure 3. Experiments using slabs of different thicknesses and channel diameters. (*a*) The force F versus displacement Δ plots 1–4 are obtained using elastic slabs having channels of diameter $d=800$ μm and thickness-to-diameter ratio $d/h=0.374$, 0.44, 0.6, 0.65, respectively. The dashed lines show that the slopes are different during loading and unloading of the slab. (*b*) Curves 1 and 2 represent the load versus displacement data for two different rates of loading, 20 and 200 μm s^{-1}, respectively. An elastic slab of $h=1240$ μm, $L=20$ mm and $d=800$ μm was used in these experiments. (*c*) Curves 1–3 represent data obtained using slabs of thickness $h=1240$ μm with embedded channels of $d=800$ μm, filled with air and liquids of viscosities $\eta=500$ and 50 000 cP, respectively.

leading to hysteresis is observed within the threshold limits $0.4<d/h<0.7$, a result observed also with other different channel diameters, $d=220$–1000 μm. Note also that the slopes of the F versus Δ curves are different during loading (c–e) and unloading (f–g), as depicted by the dashed lines in curve 3, suggesting, intuitively, that the effective rigidity of the slab decreases owing to the appearance of the kink. In fact, the sequence of images in figure 2*c–j* shows that dynamic change in the shape of the channel cross section during the loading–unloading cycle can lead to change in the flexural rigidity of the slab close to the vicinity of the channel. Importantly, in a situation of large bending, the nonlinear coupling of the geometry and the applied load results in the non-monotonic behaviour, particularly evident during unloading of the slab. These results motivate us to hypothesize that the hysteresis is elastic in origin, which we verify in the experiments in which the rate of loading and unloading of the slab is varied over an order of magnitude, from 20 to 200 μm s^{-1}. The F versus Δ data plotted in figure 3*b* shows that the rate of loading does not affect the hysteresis significantly. Furthermore, we carried out experiments with slabs having their channels filled with liquids of different viscosities, $\eta=5$–$50\,000$ mPa s, which also show no appreciable effect on the hysteresis, as shown in figure 3*c*. These results are reminiscent of similar observations during peeling off of an adhesive layer with embedded liquid-filled microchannels (Majumder *et al.* 2007), also in which case the peel strength remains independent of the viscosity of the fluid inside the channel or that of the adhesive itself. Furthermore, the experiments carried out with hydrophobic powders spread randomly on the surface of the slab and that of the channel also show no change in hysteresis signifying that adhesion and friction do not occur between surfaces during buckling of the skin, implying that the hysteresis is elastic in origin.

These observations are rationalized by scaling analysis in which we consider that the skin buckles under compressive stresses arising out of the bending of the slab. While the thickness of the skin varies from $h/2$ to $(h-d)/2$, for the sake of simple scaling, we assume that the skin is of thickness $(h-d)/2$ and the flexural rigidity (Landau & Lifshitz 1995) of which is $B=\mu h^3(1-d/h)^3/96$ where $\mu\approx1.0$ MPa is the shear modulus of the slab. It is known (Love 1944) that the skin buckles when the compressive axial load R_{av} exceeds the critical load, which is related to its length $l=d$ and bending rigidity B as $R_{\mathrm{av}}>4\pi^2B/d^2$. Substituting this in the expression for B yields

$$R_{\mathrm{av}}>4\pi^2\frac{\mu h^3(1-d/h)^3}{96d^2}. \tag{3.1}$$

In the context of the experiment in figure 2, the compressive load on the skin occurs owing to bending of the slab, which increases linearly along the thickness coordinate z as $\mu z/\rho$ where ρ is the radius of curvature of its neutral plane. In the limit of small bending, this load is integrated over the thickness of the skin to obtain an estimate of the average compressive load $\mu h^2(1-d/h)/8\rho$, which causes it to buckle. Balancing these two expressions yields the critical radius of curvature for buckling,

$$\rho_{\mathrm{c}}=\frac{3}{\pi^2}\frac{d^2/h}{(1-d/h)^2}. \tag{3.2}$$

Figure 4*a* shows that the data of ρ_{c} from the experiments with a variety of $d\sim450$–1000 μm and $h=890$–1780 μm and plotted as ρ_{c}/h indeed scales linearly with $(\bar{d}/(1-\bar{d}))^2$, where $\bar{d}=d/h$, yielding a coefficient 0.3, which corroborates well with the theoretically predicted value of $3/\pi^2$. The error bar in this figure signifies the spread of the data obtained from the experiments. It should be noted that the dependence of ρ_{c} on both d and h distinguishes itself from the wrinkling and kinking phenomena observed in similar bending experiments with solid cylinders and slabs (Gent & Cho 1999; Ghatak & Das 2007), for which the critical radius of curvature for the appearance of instability is observed to vary only with the diameter of the gel remaining independent of other material and geometric parameters of the system. Furthermore, these phenomena do not exhibit any hysteresis in the loading and unloading experiments unlike here.

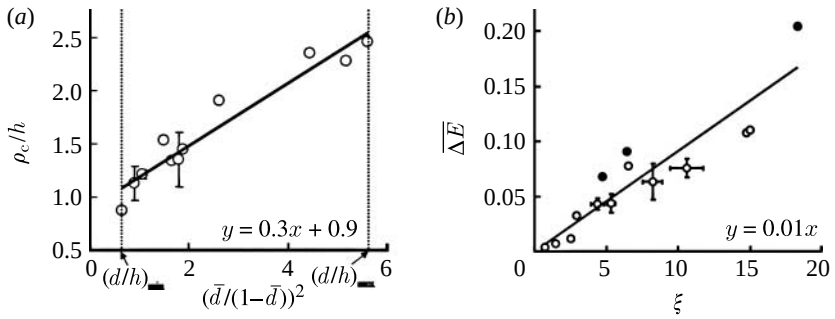

Figure 4. Critical curvature and hysteresis. (*a*) The normalized critical radius of curvature ρ_c/h, at which kink forms are plotted against the dimensionless geometric parameter $(\bar{d}/(1-\bar{d}))^2$ for various experiments with $d=450$–1000 μm and $h=890$–1800 μm. All data fall on a master line with slope 0.3. (*b*) The open symbols represent the energy hysteresis per unit width $\overline{\Delta E}$ plotted against ξ for samples of different thicknesses $h=830$–1800 μm and channel diameter $d=550$–1000 μm. The filled symbols represent the data obtained from experiments in which elastic slabs having thickness gradient but of constant channel diameter were used. Elastic slabs with $(d, h_1, h_2)=(700, 1160, 1320)$, $(800, 1380, 1630)$ and $(900, 1750, 2425)$ μm, respectively, are used in these experiments. The figure shows that all data fall on a single straight line with slope 0.01. In all these experiments, slabs of length $L=20$ mm were used.

The above analysis based on the average compressive load on the skin does not however predict that the skin should buckle inwards forming a fold inside the channel as observed in these experiments, part of the reason being the assumption of a simplified geometry. In fact, inward buckling of the skin alters the effective moment of inertia of the slab. During loading, the moment of inertia of the portion of the slab at the close vicinity of the channel is $I=(dh^3/12)(1-(12\pi/64)(d/h)^3)$, in which the length of this portion of the slab is d. However, after the thin skin undergoes buckling, the effective thickness of the slab shrinks to $h-d$, resulting in a reduced moment of inertia $I_o=(dh^3/12)(1-d/h)^3$. As a result, in order to achieve the same curvature, less bending energy is needed to be supplied. This differential energy per unit width, $\Delta E=\mu(I-I_o)/\rho_c^2$, manifests as the hysteresis in the loading–unloading cycle. Substituting in this expression the relationships of I, I_o and ρ_c, we obtain in the limit $d \ll h$ the excess energy, which is written in the dimensionless form using μd^2 as the characteristic energy, as

$$\frac{\Delta E}{\mu d^2}=\frac{9}{4}\left(\frac{h}{d}\right)^4\left(1-\frac{d}{h}+\frac{1}{8}\left(\frac{d}{h}\right)^2\right). \tag{3.3}$$

In figure 4*b*, we plot the dimensionless excess energy (open symbols) $\overline{\Delta E}=\Delta E/\mu d^2$ obtained using different slabs with respect to $\xi=(h/d)^4(1-d/h+(d/h)^2/8)$, which shows that all data fall on a master line with the result $\Delta E/\mu d^2=0.01\xi$. The data here include also those obtained in the experiments in which, instead of uniformly thick elastic slabs, the ones with thickness gradient are used. Here the thicknesses of the slabs were varied linearly from h_1 to h_2 $(h_1<h_2)$ along the width w of the slab keeping the channel of constant diameter d centrally located vertically as shown in figure 2*a*. It is easy to show that for linear gradient in thickness, the normalized excess energy per unit width varies as

$$\frac{\Delta E}{\mu d^2}=\frac{9}{4}\left(\frac{h_2}{d}\right)^4\left(\frac{1}{5}\frac{1-\bar{h}_1^5}{1-\bar{h}_1}-\frac{1}{4}\frac{d}{h_2}\frac{1-\bar{h}_1^4}{1-\bar{h}_1}+\frac{1}{24}\left(\frac{d}{h_2}\right)^2\frac{1-\bar{h}_1^3}{1-\bar{h}_1}\right), \tag{3.4}$$

where $\bar{h}_1=h_1/h_2$. The filled symbols in figure 4*b* represent the excess energy per unit width obtained from these experiments with $d=700$, 800 and 900 μm plotted against this new definition of dimensionless quantity ξ as

$$\xi=\left(\frac{h_2}{d}\right)^4\left(\frac{1}{5}\frac{1-\bar{h}_1^5}{1-\bar{h}_1}-\frac{1}{4}\frac{d}{h_2}\frac{1-\bar{h}_1^4}{1-\bar{h}_1}+\frac{1}{24}\left(\frac{d}{h_2}\right)^2\frac{1-\bar{h}_1^3}{1-\bar{h}_1}\right). \tag{3.5}$$

These data also fall on the same master curve. While the slope of the curve differs from the predicted value, which possibly is due to the over simplification of the geometry in the analysis, it captures the nonlinear dependence of the excess energy on the geometric parameters of the soft joint.

4. SUMMARY

While interlayer friction, viscous and viscoelastic dissipation have long been known to cause hysteresis in soft systems, here we showed that in purely elastic materials with embedded structures, localized deformations during cyclic loading also lead to energy dissipation. Besides shock absorption, dynamic stability and reduction in fatigue of a joint during cyclic loading, this mechanism may be important for many other situations. For example, in the context of adhesion, it has been shown earlier that 'crack arrest and initiation' during peeling off of a patterned, for example, hairy adhesive surface enhance adhesion strength (Ghatak *et al.* 2004; Chung & Chaudhury 2005; Fantner *et al.* 2005; Spolenak *et al.* 2005). There, the hysteresis is mediated by the geometry of the adhesive pad, e.g. the aspect ratio of hairs. However, here we show that in addition to geometry, the 'dynamic change in geometry' also leads to significant hysteresis. Indeed, during peeling a flexible plate off a 'microfluidic adhesive' (Majumder *et al.* 2007), the compliant thin skin over the embedded liquid-filled channels is subjected to cyclic loading and unloading, which results in the buckling of the skin and change in the channel cross section similar to our bending experiments. It will be, however, interesting to find out to what extent such buckling phenomenon can

enhance the adhesion strength of this adhesive. It should be emphasized here that while we have discussed the simple construct of a single channel oriented along the axis of bending of the elastic slab, more appropriate mimicking of the soft joints present in insects demands more elaborate designs with multiple channels of different diameters oriented differently within the elastic layer. In fact, our preliminary experiments suggest that geometric orientation of channels influences hysteresis significantly. Experiments with embedded channels spanning at an angle $\theta = 0°$–$30°$ with the axis of bending of the elastic layer show that the hysteresis is maximum for the channels oriented along the axis but decreases as $\Delta E \sim \theta^{-1/2}$ for the increase in the value of θ. Similarly, joints embedded with multiple channels arranged in parallel and series mode also affect the load–displacement plot and the resultant hysteresis. Nevertheless, the simple situation considered here drives home the point that the air pockets, blood vessels and liquid-filled glands present at the feet, wings and antennae (Krause & Dürr 2004) of many insects and invertebrates not only participate in routine metabolic activity but perhaps contribute also actively during their locomotion. This mechanism should help us design novel, multifunctional, liquid-less, soft joints for a variety of engineering applications.

A.G. acknowledges the financial assistance from the Department of Science and Technology, Government of India.

REFERENCES

Andersen, S. O. & Weis-Fogh, T. 1964 Resilin. A rubberlike protein in arthropod cuticle. *Adv. Insect. Physiol.* **2**, 1–65.

Bennet-Clark, H. C. 1975 The energetics of the jump of the locust *Schistocerca gregaria*. *J. Exp. Biol.* **63**, 53–83.

Chung, J. Y. & Chaudhury, M. K. 2005 Roles of discontinuities in bio-inspired adhesive pads. *J. R. Soc. Interface* **2**, 55–61. (doi:10.1098/rsif.2004.0020)

Dai, Z., Min, Y. & Gorb, S. N. 2006 Frictional characteristics of the beetle head–joint material. *Wear* **260**, 168–174. (doi:10.1016/j.wear.2004.12.042)

Dudek, D. M. & Full, R. J. 2006 Passive mechanical properties of legs from running insects. *J. Exp. Biol.* **209**, 1502–1515. (doi:10.1242/jeb.02146)

Fantner, G. E. *et al.* 2005 Sacrifical bonds and hidden length dissipate energy as mineralized fibrils separate during bone fracture. *Nat. Mater.* **4**, 612–616. (doi:10.1038/nmat1428)

Full, R. J. & Koditschek, D. E. 1999 Templates and anchors: neuromechanical hypotheses of legged locomotion on land. *J. Exp. Biol.* **202**, 3325–3332.

Furth, D. G. & Suzuki, K. 1992 The independent evolution of the metafemoral spring in Coleoptera. *Syst. Entomol.* **17**, 341–349. (doi:10.1111/j.1365-3113.1992.tb00555.x)

Furth, D. G., Traub, W. & Harpaz, I. 1983 What makes blepharidajump? A structural study of the metafemoral spring of a flea beetle. *J. Exp. Biol.* **227**, 43–47.

Ghatak, A. & Das, A. 2007 Kinking instability of a highly deformable elastic cylinder. *Phys. Rev. Lett.* **99**, 076101-1–076101-4. (doi:10.1103/PhysRevLett.99.076101)

Gent, A. N. & Cho, I. S. 1999 Surface instabilities in compressed or bent rubber blocks. *Rubber Chem. Technol.* **72**, 253–262.

Ghatak, A., Mahadevan, L., Chung, J. Y., Chaudhury, M. K. & Shenoy, V. 2004 Peeling from a biomimetically patterned thin elastic film. *Proc. R. Soc. A* **460**, 2725–2735. (doi:10.1098/rspa.2004.1313)

Ghatak, A., Mahadevan, L. & Chaudhury, M. K. 2005 Measuring the work of adhesion between a soft confined film and a flexible plate. *Langmuir* **21**, 1277–1281. (doi:10.1021/la0484826)

Gillett, J. D. & Wigglesworth, V. B. 1932 The climbing organ of an insect, *Rhodnius prolixus* (Hemiptera, Reduviidae). *Proc. R. Soc. B* **111**, 364–376. (doi:10.1098/rspb.1932.0061)

Gorb, S. N. 1999*a* Evolution of the dragonfly head-arresting system. *Proc. R. Soc. B* **266**, 525–535. (doi:10.1098/rspb.1999.0668)

Gorb, S. N. 1999*b* Serial elastic elements in the damselfly wing: mobile vein joints contain resilin. *Naturwissenschaften* **86**, 552–555. (doi:10.1007/s001140050674)

Grodnitsky, D. L. 1999 *Form and function of insect wings: the evolution of biological structures*. Baltimore, MD: The Johns Hopkins University Press.

Gronenberg, W. 1996 Fast actions in small animals: springs and click mechanisms. *J. Comp. Physiol. A* **178**, 727–734. (doi:10.1007/BF00225821)

Haas, F., Gorb, S. & Wootton, R. J. 2000 Elastic joints in dermapteran hind wings: materials and wing folding. *Arthropod Struct. Dev.* **29**, 137–146. (doi:10.1016/S1467-8039(00)00025-6)

Hyon, S.-Ho., Hale, J. G. & Cheng, G. 2007 Full-body compliant human–humanoid interaction: balancing in the presence of unknown external forces. *IEEE Trans. Robot.* **23**, 884–898. (doi:10.1109/TRO.2007.904896)

Krause, A. F. & Dürr, V. 2004 Tactile efficiency of insect antennae with two hinge joints. *Biol. Cybern.* **91**, 168–181. (doi:10.1007/s00422-004-0490-6)

Landau, L. D. & Lifshitz, E. M. 1995 *Theory of elasticity*, vol. 7. Oxford, UK: Butterworth-Heinemann.

Love, A. E. H. 1944 *A treatise on the mathematical theory of elasticity*, 4th edn. New York, NY: Dover.

Majumder, A., Ghatak, A. & Sharma, A. 2007 Microfluidic adhesion induced by sub-surface micro-structures. *Science* **318**, 258–261. (doi:10.1126/science.1145839)

Sane, S. P., Dieudonné, A., Willis, M. A. & Daniel, T. L. 2007 Antennal mechanosensors mediate flight control in moths. *Science* **315**, 863–866. (doi:10.1126/science.1133598)

Shimoyama, I., Miura, H., Suzuki, K. & Ezura, Y. 1993 Insect-like microrobots with external skeletons. *Cont. Syst. Mag. IEEE* **13**, 37–41. (doi:10.1109/37.184791)

Spolenak, R., Gorb, S., Gao, H. & Arzt, E. 2005 Effects of contact shape on the scaling of biological attachments. *Proc. R. Soc. A* **461**, 305–319. (doi:10.1098/rspa.2004.1326)

Ting, L. H., Blickhan, R. & Full, R. J. 1994 Dynamic and static stability in hexapedal runners. *J. Exp. Biol.* **197**, 251–269.

Verma, M. K. S., Majumder, A. & Ghatak, A. 2006 Embedded template-assisted fabrication of complex microchannels in PDMS and design of a microfluidic adhesive. *Langmuir* **22**, 10 291–10 295. (doi:10.1021/la062516n)